Impact Factor:					
	ISRA (India) = 6.317	SIS (USA) = 0.912	ICV (Poland) = 6.630
	ISI (Dubai, UAE) = 1.582	РИНЦ (Russia) = 3.939	PIF (India) = 1.940
	GIF (Australia) = 0.564	ESJI (KZ) = 8.771	IBI (India) = 4.260
	JIF = 1.500	SJIF (Morocco) = 7.184	OAJI (USA) = 0.350

SOI: 1.1/TAS DOI: 10.15863/TAS

International Scientific Journal

Theoretical & Applied Science

p-ISSN: 2308-4944 (print) **e-ISSN:** 2409-0085 (online)

Year: 2023 **Issue:** 05 **Volume:** 121

Published: 24.05.2023 **http://T-Science.org**

Issue Article

Normurod Ibodullayevich Fayzullayev
Samarkand State University
Doctor of Technical Sciences, Professor, Department of Polymer Chemistry and Chemical Technology,
140104, Samarkand, Republic of Uzbekistan
https://orcid.org/0000-0001-5838-3743
fayzullayev72@inbox.ru

Mashrab Abdumalikovich Mamirzayev
Samarkand State University
Researcher, Department of Polymer Chemistry and Chemical Technology,
140104, Samarkand, Republic of Uzbekistan
E-mail: mashrab87@mail.ru

Davron Abror Ogli Asrorov
Samarkand State University
Master's Degree Student,
140104, Samarkand, Republic of Uzbekistan

PREPARATION OF MESOPOROUS CARBON FROM NATURAL GAS

Abstract: *In this work, kinetic relations of carbon deposition on the surface of a methane catalyst 10%Ni·5%Co·5%Fe·10%Cu/MgO, 5%Ni·5%Co·5%Fe·15%Cu/MgO and 15%Ni·5%Co·5%Fe· 5%Cu·2%Mo/MgO were studied. As a result of the research, the efficiency of the 15%Ni·5%Co·5%Fe·5%Cu·2%Mo/MgO catalyst in natural gas decomposition reactions has been shown. During the decomposition of natural gas into hydrogen and mesoporous carbon in the presence of a 15%Ni·5%Co·5%Fe·5%Cu·2%Mo/MgO catalyst, the following data were obtained: the volumetric flow rate of natural gas at a productivity of 20,000 h^{-1}, the optimal range temperatures 700÷725 °C. The yield of hydrogen from 1 g of the catalyst is 600÷650 l, and mesoporous carbon reaches 160 g/g. The hydrogen concentration at the outlet of the reactor is 70-75 mol.%.*

Key words: *methane, natural gas, hydrogen, mesoporous carbon, reaction yield, conversion, catalyst.*

Language: *English*

Citation: Fayzullayev, N. I., Mamirzayev, M. A., & Asrorov, D. A. (2023). Preparation of Mesoporous Carbon from Natural Gas. *ISJ Theoretical & Applied Science, 05 (121),* 301-313.

Soi: http://s-o-i.org/1.1/TAS-05-121-45 ***Doi***: https://dx.doi.org/10.15863/TAS.2023.05.121.45

Scopus ASCC: *1600.*

Introduction

The amount of gases released as a result of the combustion of petroleum satellite gas is 0.5 million tons per year [1]. Combustion of petroleum gas causes thermal pollution of the environment [1-3].

Oil and gas industry facilities have various ecologically significant harmful effects [4-7]. In this case, both natural hydrocarbons and their processing products, various reagents, alkalis, acids, substances formed during combustion, etc. can enter the environment. Environmental safety must be ensured in all areas of the oil and gas complex [8,9].

The toxic effect of carbon monoxide is related to the haemoglobin in the blood, which converts it into carboxyhemoglobin, which cannot transport oxygen from the lungs to the tissues [7,10].

There are several options for the disposal of petroleum satellite gas other than direct flaring. Among these options, the direct use of petroleum satellite gas and its processing can be highlighted [1, 11-14].

In addition, it is possible to organize the production of motor fuel in the mines, as well as to develop the gas-chemical industry and to obtain new

products from oil and gas raw materials [6, 7, 15-17]. All three methods above can provide disposal of 95-98% of the gas obtained. Gas injection into oil reservoirs is used in cases where gas processing or utilization possibilities are limited. However, this is a very irrational use of resources, as a significant amount of valuable petrochemical raw materials is lost. The second and third methods of disposal are relatively economical because they do not require the construction of a complete cycle of gas collection, transportation and processing facilities.

Currently, a large number of carbon materials with different structures are known, among which mesoporous carbon occupies a special place. Mesoporous carbon is formed by the decomposition of hydrocarbons in the presence of catalysts containing transition metals of the iron subgroup. These materials are of great practical interest due to their unique textural and physicochemical properties [24, 25].

Experimental part

To study the kinetics of nanocarbon extraction, a flow reactor with an inner diameter of 60 mm and a length of 400 mm, filled with a nozzle of 100 mm for uniform heating of the injected gas mixture and equipped with a nozzle for introducing gas from the bottom side, was assembled. During the process, the mass change was monitored on a torsion balance. The reactor was heated by an electric furnace, the temperature of which was controlled using a laboratory autotransformer. Temperature control in the reactor was carried out using a calibrated chromed-aluminium thermocouple and a millivoltmeter located inside the reactor.

The specific surface area of nanocarbon(S_{sol}) and porosity (G')using the Brunauer-Emmett-Teller (BET) method. It was determined by low-temperature nitrogen adsorption on an ASAP 2020 instrument from Micromeritics (USA). Nitrogen adsorption-desorption isotherms were recorded at a temperature of 77 K in the relative pressure range P/P_s = 0.0–1.0. The value of Ssol was estimated by the BET method based on the adsorption isotherm at P/P_s = 0.05-0.30. The size of mesopores and their size distribution using the Barrett, Joyner and Halenda (BJH) method at P/Ps = 0.35-0.95, for micropores these parameters are nitrogen adsorption in the range P/P_s = 0.00 ÷ 0.01 - found through the desorption isotherm.

X-ray phase analysis was performed on a DRON-5M diffractometer, characteristic radiation of copper filtered with a nickel filter (Ka line), 20 kV imaging mode. Structural and morphological properties of carbon were studied using scanning and illumination electron microscopes. A JSM-6460 microscope was used for scanning electron microscopy. Transmission electron microscopic (EEM) images were taken using a JYeOL JYeM-2010 electron microscope. The illumination electron microscope operates at an accelerating voltage of 200 kV and has a grid size of 0.14 nm. The derivatographic analysis was carried out in the atmosphere of F. Pulik, Y. Paulik and L. Erdey in the derivatograph system at the temperature of raising the temperature from 1 to 10 ℃/min.

A filter based on zeolite was used to clean gas mixtures from impurities and dry them from moisture. The qualitative and quantitative composition of gas substances of the reaction was analyzed by the gas chromatographic method in the "Chromatek-Crystal 7000" chromatograph.

The yield of nanocarbon was determined using the following formula:

$$X_{HU} = (m_{KOH} - m_{bosh})/m_{bosh})$$

Here X_{NU} is nanocarbon yield, g/g_{cat}; m_{bosh} - mass of the sample before the start of the experiment, g; m_{bosh} is the mass of the sample at the end of the experiment, g.

Results and discussion

It is known from previous studies that 5%Ni·5%Co·5%Fe·15%Cu/MgO catalysts are very active and stable enough in the decomposition reaction of methane to hydrogen and mesoporous carbon. Therefore, the catalytic properties of these catalysts were investigated for the first time in the decomposition of methane at different temperatures in a McBean scale flow reactor. Figure 1 shows the kinetic curves of carbon deposition on the catalyst surface from methane on 5%Ni·5%Co·5%Fe·15%Cu/MgO catalyst at different temperatures.

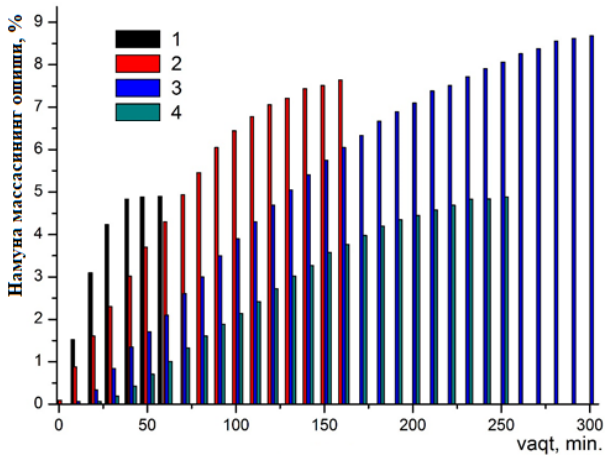

Figure 1. Kinetic curves of carbon deposition from methane on catalyst surface in 5%Ni·5%Co·5%Fe·15%Cu/MgO catalyst at different temperatures: 1 – 700 ℃, 2 – 650 ℃, 3 – 600 ℃, 4 – 550 ℃.

Figure 1 shows that the optimum temperatures for methane decomposition reaction in the presence of 5%Ni·5%Co·5%Fe·15%Cu/MgO catalyst are 600÷650℃. The reaction stability of these catalysts decreases at temperatures above 650℃.

Figure 2 shows an electron microscopic photograph of mesoporous carbon formed from methane at 700℃ on 5%Ni·5%Co·5%Fe·15%Cu/MgO catalyst.

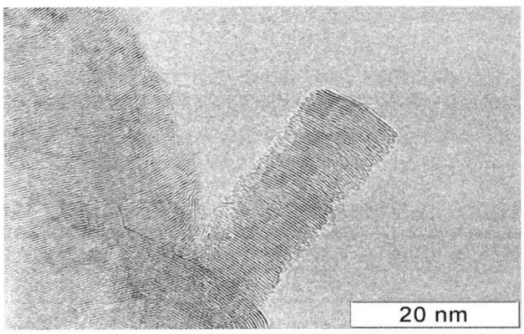

Figure 2. Electron micrograph of mesoporous carbon formed from methane at 700℃ on 5%Ni·5%Co·5%Fe·15%Cu/MgO catalyst

However, despite the high activity and stability of the 5%Ni·5%Co·5%Fe·15%Cu/MgO catalyst in the methane decomposition reaction, high methane conversion cannot be achieved with this catalyst due to thermodynamic limitations. Figure 3 shows the temperature dependence of the equilibrium concentration of hydrogen for the reaction of decomposition of methane into hydrogen and carbon. It follows from this indicator that the area of average temperatures (500÷750℃). Therefore, the problem of increasing the stability of the catalyst by further increasing the working temperature has arisen.

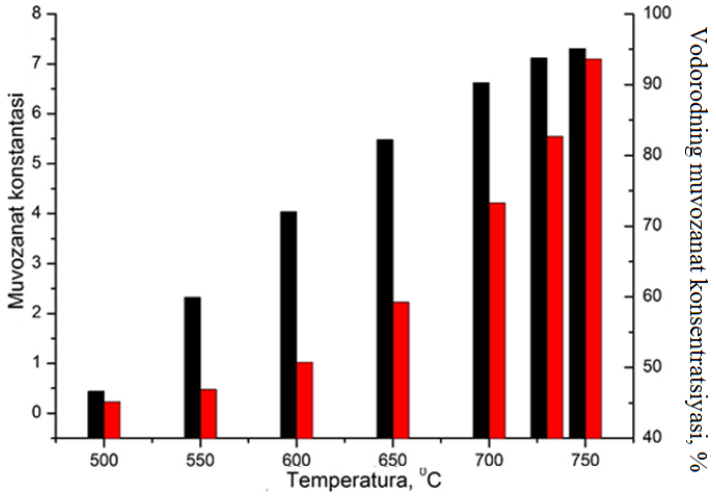

Figure 3. The equilibrium constant for the decomposition reaction and the temperature dependence of the equilibrium concentration of hydrogen.$CH_4 \rightarrow 2H_2 + C$

In improving the composition of the 5%Ni·5%Co·5%Fe·15%Cu/MgO catalyst, we started from theoretical concepts based on the carbide cycle mechanism of carbon formation in iron subgroup metals. It is known that mesoporous carbon grows on highly dispersed nickel particles by the carbide cycle mechanism. Mass transfer of carbon atoms occurs through their diffusion from the place of formation to the centres of crystallization through the volume of metal particles. It follows from the mechanism of the carbide cycle that the distribution of carbon atoms occurs under the influence of a concentration gradient. This gradient is huge. The presence of a high degree of saturation at the front of the metal particle in contact with the gas phase makes the system unstable. As a result, gradual changes occur in the structure of Ni-Su-Co-Fe alloy particles. A crystal particle with a clear cross-section is transformed into a macroblock under the influence of carbon diffusion flow. Carbon accumulates both on the boundaries of the blocks and on the planes of contact with them. Fragmentation of particles causes them to disperse in space into smaller particles that are quickly deactivated. A further increase in the amount of iron eliminates the carbon concentration gradient in the catalytically active particle, which occurs both due to the decrease in the rate of methane decomposition at the front of the metal particle and the need to increase the rate of removal of carbon atoms from the front of the metal particle. The diffusion coefficient of carbon atoms through the volume of metallic iron is almost three times greater than the diffusion coefficient through the volume of metallic nickel,

In fact, the modification of 5%Ni·5%Co·5%Fe·15%Cu/MgO with iron leads to a decrease in the methane decomposition reaction rate. Figure 4 shows 10%Ni·5%Co·5%Fe·10%Cu/MgO (1), 5%Ni·5%Co·5%Fe·15%Cu/MgO (2) and 15%Ni·5 %Co·5%Fe·5%Cu·2%Mo/MgO (3) catalysts shows the kinetic curves of carbon deposition on the catalyst surface from methane at 700 °C. As mentioned above, the stability of 5%Ni·5%Co·5%Fe·15%Cu/MgO catalyst working at 700°C is almost doubled compared to working at 600÷650°C. Although the performance stability of the 5%Ni·5%Co·5%Fe·15%Cu/MgO catalyst is much higher than that of the 10%Ni·5%Co·5%Fe·10%Cu/MgO catalyst (1), this catalyst is also deactivated after 40 minutes. Figure 4 shows that

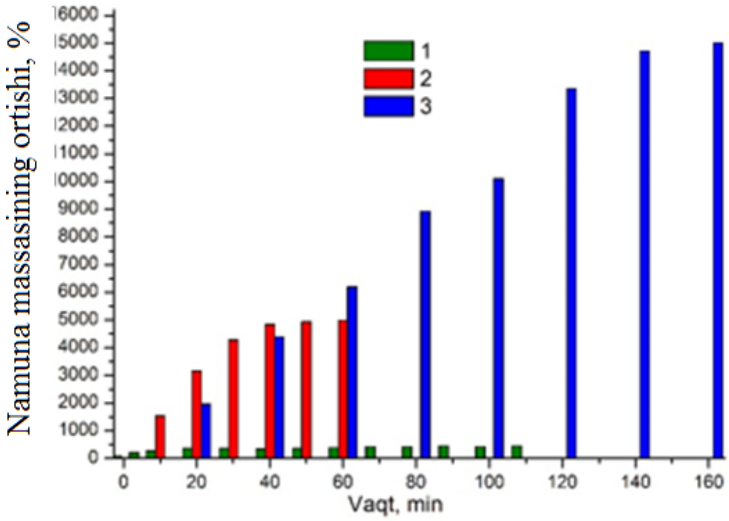

Figure 4. 10%Ni·5%Co·5%Fe·10%Cu/MgO (1), 5%Ni·5%Co·5%Fe·15%Cu/MgO (2) and 15%Ni·5 at 700°C %Co·5%Fe·5%Cu·2%Mo /MGO (3) kinetic curves of carbon deposition on the catalyst surface from methane

In Table 1, 10%Ni·5%Co·5%Fe·10%Cu/MgO, 5%Ni·5%Co·5%Fe·15%Cu/MgO and 15%Ni·5%Co·5%Fe Comparative data on the formation of mesoporous carbon during methane decomposition at 700°C for 1 h in the presence of ·5%Cu·2%Mo/ MgO catalysts are presented. The increase in sample mass occurs due to the formation of mesoporous carbon in the catalyst.

Table 1. Formation of mesoporous carbon on nickel catalysts during methane decomposition. The temperature is 700 °C.

Catalyst	Increase in mass of the sample during 1 hour, wt.%
10%Ni·5%Co·5%Fe·10%Cu/MgO	310
5%Ni·5%Co·5%Fe·15%Cu/MgO	4,900
15%Ni·5%Co·5%Fe·5%Cu·2%Mo/ MgO	6 400

Figure 5 shows the kinetic curves of methane carbon deposition in the presence of 15%Ni·5%Co·5%Fe·5%Cu·2%Mo/ MgO catalyst in the temperature range of 700-750 °C. It can be seen that the stability of mesoporous carbon growth in 15%Ni·5%Co·5%Fe·5%Cu·2%Mo/ MgO catalyst is maintained in this temperature range.

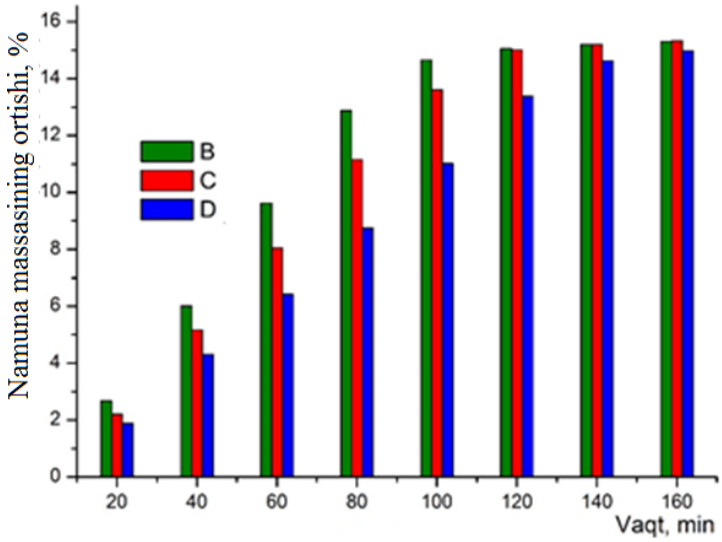

Figure 5. Kinetic curves of carbon deposition formed during the decomposition of methane at different temperatures in the presence of 15%Ni·5%Co·5%Fe·5%Cu·2%Mo/MgO catalyst, at temperatures: 1 – 750 °C; 2 – 725 °C; 3 – 700 °C.

Figure 5 shows that the modification of 5%Ni·5%Co·5%Fe·15%Cu/MgO catalyst with iron additives increased the optimum operating temperature to 700–750 °C while maintaining high catalyst stability. The production efficiency of mesoporous carbon in the modified 15%Ni·5%Co·5%Fe·5%Cu·2%Mo/MgO catalyst at 700-750 °C was 150-160 g/g.

Mesoporous carbon is formed simultaneously on several faces of the alloy particles (Fig. 6).

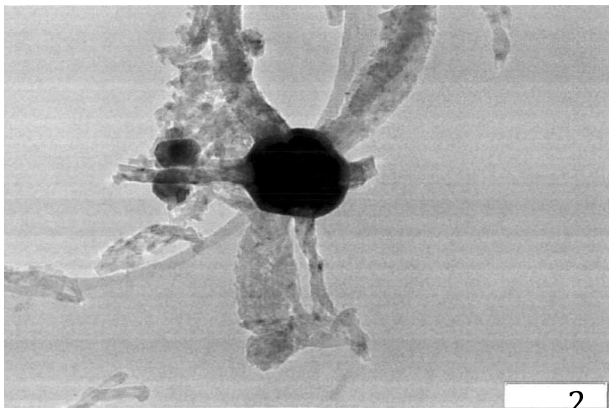

Figure 6. Mesoporous carbon obtained from the decomposition of methane on 15%Ni·5%Co·5%Fe·5%Cu·2%Mo/MgO catalyst at 700°C.

Figure 7 shows that the kinetic curves of carbon deposition on the catalyst surface from methane and natural gas for the 15%Ni·5%Co·5%Fe·5%Cu·2%Mo/MgO catalyst are close to each other. It should be noted that the decrease in catalytic activity in natural gas begins a little earlier than in pure methane.

If we focus only on obtaining hydrogen as a reaction product, then additional hydrogen can be obtained by adding a catalyst regeneration step to the process. In this case, the carbonized catalyst must be regenerated with steam.

Since the evaluation of possible methane conversion is based on the assumption that the 15%Ni·5%Co·5%Fe·5%Cu·2%Mo/MgO catalyst provides stable operation with near-equilibrium methane conversion, it is experimentally tested interesting to see. In this regard, experiments were conducted on splitting natural gas in a flow reactor.

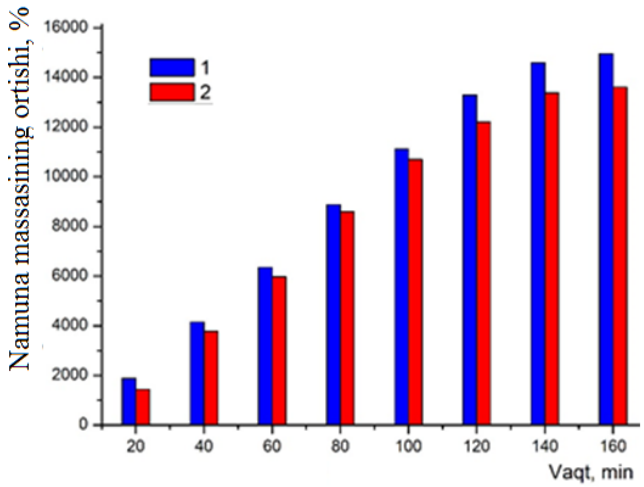

Figure 7.Kinetic curves of carbon deposition on catalyst surface on 15%Ni·5%Co·5%Fe·5%Cu·2%Mo/MgO catalyst from methane (1) and natural gas (2) at T = 700 °C.

Experiments were conducted with natural gas at a temperature of 700 °C. 15%Ni·5%Co·5%Fe·5%Cu·2%Mo/MgO catalyst 0.5 g was obtained, natural gas transfer rate - 10 l/h. Under these conditions, the 15%Ni·5%Co·5%Fe·5%Cu·2%Mo/MgO catalyst was found to provide a more stable reaction over 28 h (Figure 8). Natural gas (methane) conversion reaches a steady state within half an hour and remains at approximately 55% for 28 hours.

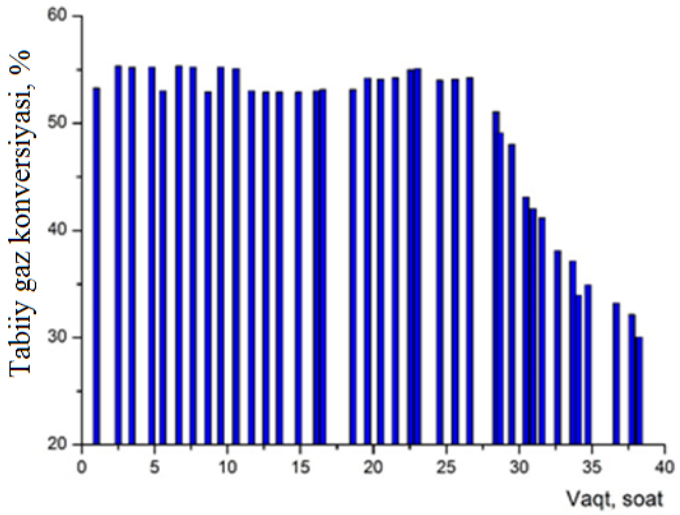

Figure 8. Time dependence of natural gas conversion.

The reaction temperature is 700 °C. Natural gas transfer rate - 10 l/hour.

15%Ni·5%Co·5%Fe·5%Cu·2%Mo/MgO catalyst mass - 0.5 g.

Figure 9 shows the hydrogen concentration (%) at the reactor outlet as a function of time. During the stationary period of the reaction, the hydrogen concentration at the outlet of the reactor was about 70%. The dashed lines show the equilibrium level of hydrogen concentration. Therefore, during the stationary period of the reaction, the hydrogen concentration at the outlet of the reactor is approximately 15% lower than the equilibrium state.

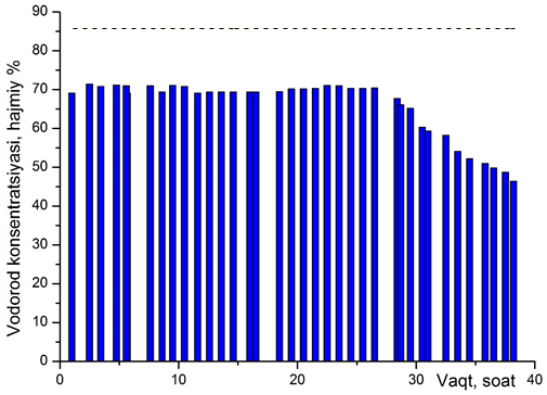

Figure 9. Graph of hydrogen concentration (%) at reactor outlet versus time. The reaction temperature is 700 °C. Natural gas supply – 10 l/h. The mass of 15%Ni·5%Co·5%Fe·5%Cu·2%Mo/MgO catalyst is 0.5 g. The dashed lines show the equilibrium hydrogen concentration levels.

Table 2 presents mesoporous carbon and hydrogen recovery process data during natural gas decomposition in a continuous impactor during steady operation over a 15%Ni·5%Co·5%Fe·5%Cu·2%Mo/MgO catalyst.

Table 2.Natural gas decomposition process data in a continuous impact device at 700°C on 15%Ni·5%Co·5%Fe·5%Cu·2%Mo/MgO catalyst

Process parameters	Value
15%Ni·5%Co·5%Fe·5%Cu·2%Mo/MgO catalyst mass	0.5 g
Natural gas flow rate to the reactor	10 l/h
Natural gas conversion	60%
Hydrogen concentration at the exit of the reactor	72 per cent
The concentration of the mixture of C2-C3 hydrocarbons at the exit of the reactor	~ 0.4 %
Performance of mesoporous carbon	4.5 gC/gkat·h
Mass of carbon produced during the overall process	78 g

The concentration of C_2-C_3 hydrocarbon compounds at the outlet of the reactor decreased by more than an order of magnitude, and their total concentration at the outlet of the reactor did not exceed 0.3%. 78 g of carbon was formed on the catalyst in 38 hours. Carbon yield from 1 g of catalyst was 156 g of mesoporous carbon. It was previously shown that the yield of mesoporous carbon was 136 g/g at 700 °C using a 15%Ni·5%Co·5%Fe·5%Cu·2%Mo/MgO catalyst in a McBean scale reactor. Thus, the efficiency of mesoporous carbon in the rotating reactor installation is higher than that of the McBean reactor.

Figure 10 shows the time dependence of the hydrogen concentration (%) at temperatures of 700-750 °C.

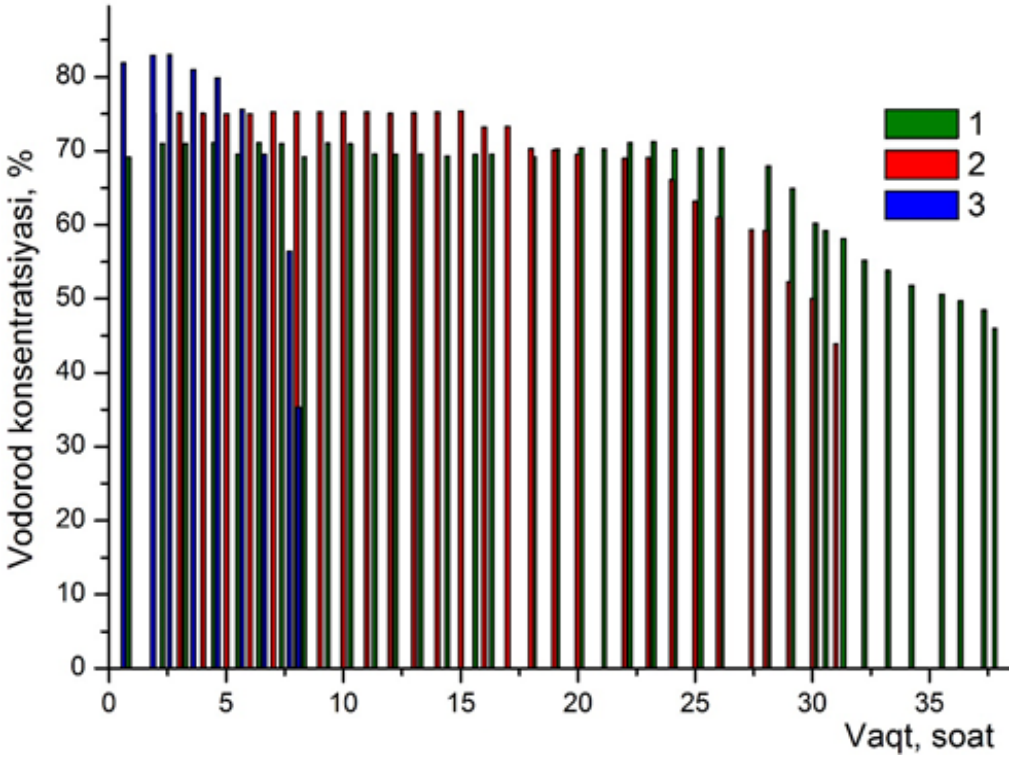

Figure 10.Time dependence of hydrogen concentration (%) at different temperatures: 1 – 700 ℃; 2 – 725 ℃; 3 – 750 ℃. Natural gas supply rate - 10 l/h. The mass of 15%Ni·5%Co·5%Fe·5%Cu·2%Mo/MgO catalyst is 0.5 g.

Figure 10 shows that the hydrogen concentration at the reactor outlet increases with increasing temperature. If during the stationary period of the reaction, the hydrogen concentration at the exit from the reactor at a temperature of 700 ℃ is about 70%, at a temperature of 725 ℃ - 75%, and at 750 ℃ it increases to 82÷84%. However, as the reaction temperature increased, the stability of the catalyst decreased. Stationary reaction time at 750℃ was 4-5 hours. A brief description of natural gas cracking in a continuous unit is given in Table 3.

Table 3. Natural gas cracking process parameters in a continuous plant on 15%Ni·5%Co·5%Fe·5%Cu·2%Mo/MgO catalyst at 700-750 ℃

Process parameters	Reaction temperature, ℃		
	700	725	750
Hydrogen output concentration, %	70%	75%	83%
Stable working hours, hours	28	15	4

Adsorption separation of hydrogen from the hydrogen-methane mixture. The conducted studies showed that the amount of S_2-S_4 hydrocarbons at the outlet of the reactor is 1÷2 mol%. In this regard, the main focus of the work was on the separation of the methane-hydrogen mixture. Good results were achieved using the adsorption method.

The adsorbent (activated carbon, 12÷13 g) was poured into a quartz adsorber placed in a Dewar's vessel. A Dewar flask is filled with a cooling mixture. The decan was cooled to a specified temperature with liquid nitrogen. Adsorption was carried out in the temperature range from room temperature to -30℃, and solid and liquid decane were obtained. At the entrance to the adsorber, a mixture of hydrogen and methane was delivered at a total rate of 10 l/h. The amount of methane in the mixture is 10 vol.%. The gas at the outlet of the adsorber was analyzed every 2 minutes using a "Crystal 4000" chromatograph.

Table 4 shows the characteristics of the pore structure parameters of the active carbons used in the work. As can be seen from the table, SKT-2A coal has the largest volume of micropores.

Initially, the experiments were conducted at a temperature of 15 ℃. At the entrance to the adsorber, a mixture of hydrogen and methane was supplied at a rate of 10 l/h. The amount of methane in the mixture was 10 vol.%. All the activated carbons examined in this study showed poor results. In the case of AGN-2, CG-48A, methane was observed at the adsorber outlet

after 1-2 minutes. The best results were achieved on SKT-2A activated carbon. Therefore, the adsorption studies for this coal were conducted at low temperatures from 0 ℃ to -30 ℃.

Table 4. Parameters of the porous structure of activated carbon

Pore volume, cm3/g	Activated charcoal brand		
	AGN-2	CG-48A	SKT-2A
Total pore volume	0.6...0.73	0.7	0.75...0.80
Micropore	0.32...0.35	0.30...0.32	0.37...0.42
Mesoporous	0.05...0.06	0.05...0.08	0.18...0.22

We used the following types of activated carbon: AGN-2, CG-48A and SKT-2A. It has been shown experimentally that as the temperature of the adsorber decreases, the sorption capacity of activated carbon for methane increases. Experimental data SKT-2A activated carbon at 0℃, It was used to calculate the dynamic adsorption capacity at temperatures of -10℃, -20℃ and -30℃. Table 5 shows the calculated data of the dynamic adsorption capacity of SKT-2A activated carbon at different temperatures.

Table 5. The dynamic adsorption capacity of SKT-2A activated carbon for different temperatures

	Value			
Adsorption temp	0 ℃	-10℃	-20℃	-30℃
Dynamic capacity	0.5%	0.7%	0.9%	1.5%

Thus, the principle possibility of hydrogen purification from methane was demonstrated. Among the studied active carbons (AGN-2, CG-48A, SKT-2A), the best results were obtained with SKT-2A activated carbon. Studies on the effect of adsorption temperature have shown that when the adsorber temperature decreases from 0 to -30 ℃, the sorption capacity of activated carbon for methane increases from 0.5 to 1.5 wt.%.

Morphology of natural gas-derived mesoporous carbon. Figure 10 shows an electron microscopic photograph of mesoporous carbon formed from methane on 15%Ni·5%Co·5%Fe·5%Cu·2%Mo/MgO catalyst at 700 ℃. Most of the tubes are about 10÷30 nm in size, but as you can see, there are also a few nanotubes with larger diameters.

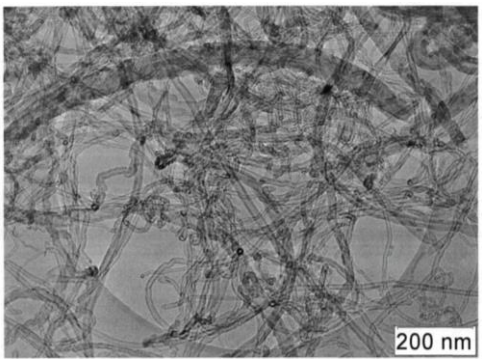

Figure 10.Electron microscopic photograph of mesoporous carbon formed from methane at 700℃ on 15%Ni·5%Co·5%Fe·5%Cu·2%Mo/MgO catalyst

In the presented picture, the structure of the carbon nanotube (graphite layers and the space inside) is clearly visible (Fig. 11).

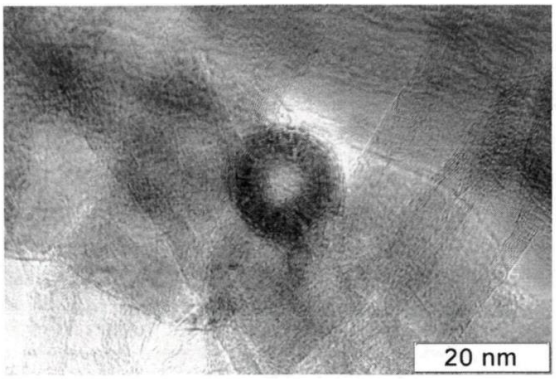

Figure 11.Electron microscopic photograph (high magnification) of mesoporous carbon formed from methane on 15%Ni·5%Co·5%Fe·5%Cu·2%Mo/MgO catalyst at 700 °C.

The addition of molybdenum oxide results in the growth of tubes that are smaller in diameter and closer in size. As can be seen in the photo (Fig. 12), the diameter is 5÷20 nm.

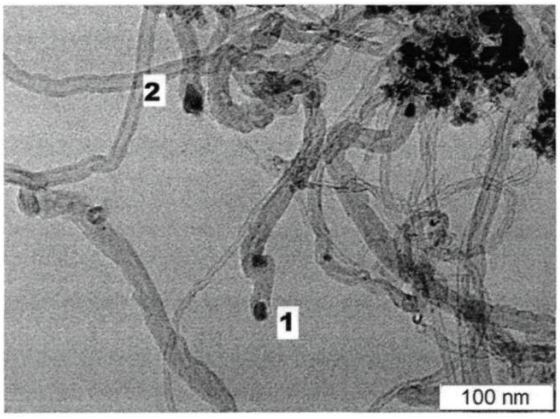

Figure 12. Morphology of mesoporous carbon on 15%Ni·5%Co·5%Fe·5%Cu·2%Mo/MgO catalyst at 750 °C. Particles used for microanalysis are marked with numbers 1 and 2.

EDX studies have shown that metal particles catalyzing the growth of mesoporous carbon from natural gas in 15%Ni·5%Co·5%Fe·5%Cu·2%Mo/MgO catalysts are nickel, copper, iron, consisting of cobalt and molybdenum.

According to the results of microanalysis, it was found that the diameter of catalytically active particles and, accordingly, the diameter of mesoporous carbon decreases with increasing molybdenum content because an increase in the content of molybdenum in approximately the same cobalt content leads to a significant decrease in the diameter of catalytically active nanoparticles.

Kinetic studies of catalysts allowed us to determine the optimal composition of the catalyst - it is 15%Ni·5%Co·5%Fe·5%Cu·2%Mo /MGO, electron microscopic studies showed that mesoporous carbon in this catalyst is coaxial-cylindrical structure is formed.

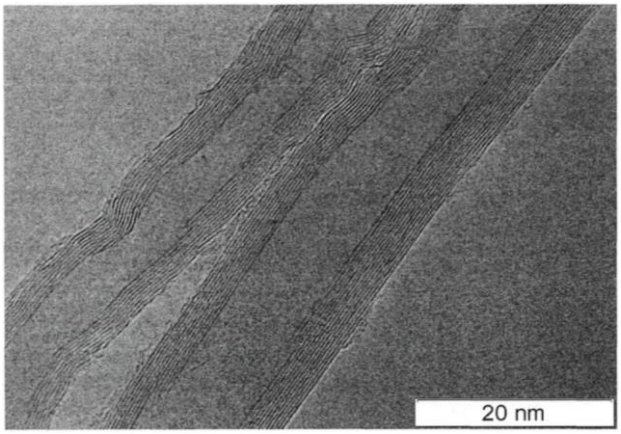

Figure 13.Electron microscopic photograph of natural gas-derived mesoporous carbon on 15%Ni·5%Co·5%Fe·5%Cu·2%Mo/MgO catalyst at 700°C

Conclusion

As a result of the conducted research, the efficiency of 15%Ni·5%Co·5%Fe·5%Cu·2%Mo/MgO catalyst in natural gas cracking reactions was shown. The following data were obtained during the decomposition of natural gas into hydrogen and mesoporous carbon in a rotary reactor continuous impact device with 15%Ni·5%Co·5%Fe·5%Cu·2%Mo/MgO catalyst: natural gas volume flow At a speed of 20000 h-1, the optimal temperature range is 700÷725 °C. The output of hydrogen is 600÷650 litres from 1 g of catalyst, and 160 g/g in the case of mesoporous carbon. The concentration of hydrogen at the outlet of the reactor is 70-75 mol%.

References:

1. Terrones, M. (2003). Science and technology of the twenty-first century: synthesis, properties, and applications of carbon nanotubes. *Annual review of materials research*, 33(1), 419-501.
2. Ding, S., Xiang, Y., Ni, Y. Q., Thakur, V. K., Wang, X., Han, B., & Ou, J. (2022). In-situ synthesizing carbon nanotubes on cement to develop self-sensing cementitious composites for smart high-speed rail infrastructures. *Nano Today*, 43, 101438.
3. Zhou, X., Wang, Y., Gong, C., Liu, B., & Wei, G. (2020). Production, structural design, functional control, and broad applications of carbon nanofiber-based nanomaterials: A comprehensive review. *Chemical Engineering Journal*, 402, 126189.
4. Bai, Y., Yue, H., Wang, J., Shen, B., Sun, S., Wang, S., ... & Wei, F. (2020). Super-durable ultralong carbon nanotubes. *Science*, 369(6507), 1104-1106.
5. Hills, G., Lau, C., Wright, A., Fuller, S., Bishop, M. D., Srimani, T., ... & Shulaker, M. M. (2019). Modern microprocessor built from complementary carbon nanotube transistors. *Nature*, 572(7771), 595-602.
6. Kumar, S., Saeed, G., Zhu, L., Hui, K. N., Kim, N. H., & Lee, J. H. (2021). 0D to 3D carbon-based networks combined with pseudocapacitive electrode material for high energy density supercapacitor: A review. *Chemical Engineering Journal*, 403, 126352.
7. Rao, R., Pint, C. L., Islam, A. E., Weatherup, R. S., Hofmann, S., Meshot, E. R., ... & Hart, A. J. (2018). Carbon nanotubes and related nanomaterials: critical advances and challenges for synthesis toward mainstream commercial applications. ACS nano, 12(12), 11756-11784.
8. Pinilla, J. L., De Llobet, S., Moliner, R., & Suelves, I. (2017). Ni-Co bimetallic catalysts for the simultaneous production of carbon nanofibres and syngas through biogas decomposition. *Applied Catalysis B: Environmental*, 200, 255-264.
9. Gómez-Pozuelo, G., Pizarro, P., Botas, J. A., & Serrano, D. P. (2021). Hydrogen production by catalytic methane decomposition over rice husk derived silica. *Fuel*, 306, 121697.
10. Fan, Z., Weng, W., Zhou, J., Gu, D., & Xiao, W. (2021). Catalytic decomposition of methane to

produce hydrogen: A review. *Journal of Energy Chemistry*, 58, 415-430.

11. Dipu, A. L. (2021). Methane decomposition into COx-free hydrogen over a Ni-based catalyst: an overview. *International Journal of Energy Research*, 45(7), 9858-9877.
12. Qian, J. X., Chen, T. W., Enakonda, L. R., Liu, D. B., Basset, J. M., & Zhou, L. (2020). Methane decomposition to pure hydrogen and carbon nano materials: State-of-the-art and future perspectives. *International Journal of Hydrogen Energy*, 45(32), 15721-15743.
13. Sánchez-Bastardo, N., Schlögl, R., & Ruland, H. (2020). Methane pyrolysis for co2-free h2 production: A green process to overcome renewable energies unsteadiness. *Chemie Ingenieur Technik*, 92(10), 1596-1609.
14. Cazaña, F., Latorre, N., Tarifa, P., Labarta, J., Romeo, E., & Monzón, A. (2018). Synthesis of graphenic nanomaterials by decomposition of methane on a Ni-Cu/biomorphic carbon catalyst. Kinetic and characterization results. *Catalysis Today*, 299, 67-79.
15. Lin, X., Zhu, H., Huang, M., Wan, C., Li, D., & Jiang, L. (2022). Controlled preparation of Ni–Cu alloy catalyst via hydrotalcite-like precursor and its enhanced catalytic performance for methane decomposition. *Fuel Processing Technology*, 233, 107271.
16. Tezel, E., Figen, H. E., & Baykara, S. Z. (2019). Hydrogen production by methane decomposition using bimetallic Ni–Fe catalysts. *International Journal of Hydrogen Energy*, 44(20), 9930-9940.
17. Henao, W., Cazaña, F., Tarifa, P., Romeo, E., Latorre, N., Sebastian, V., ... & Monzón, A. (2021). Selective synthesis of carbon nanotubes by catalytic decomposition of methane using Co-Cu/cellulose derived carbon catalysts: A comprehensive kinetic study. *Chemical Engineering Journal*, 404, 126103.
18. Cazaña, F., Latorre, N., Tarifa, P., Royo, C. J., Sebastián, V., Romeo, E., ... & Monzón, A. (2022). Performance of AISI 316L-stainless steel foams towards the formation of graphene related nanomaterials by catalytic decomposition of methane at high temperature. *Catalysis Today*, 383, 236-246.
19. Karaeva, A. R., Urvanov, S. A., Kazennov, N. V., Mitberg, E. B., & Mordkovich, V. Z. (2020). Synthesis, structure and electrical resistivity of carbon nanotubes synthesized over group VIII metallocenes. *Nanomaterials*, 10(11), 2279.
20. Venkataraman, A., Amadi, E. V., Chen, Y., & Papadopoulos, C. (2019). Carbon nanotube assembly and integration for applications. *Nanoscale research letters*, 14(1), 1-47.
21. Amara, H., & Bichara, C. (2019). Modeling the growth of single-wall carbon nanotubes. *Single-Walled Carbon Nanotubes: Preparation, Properties and Applications*, 1-23.
22. Li, M., Liu, X., Zhao, X., Yang, F., Wang, X., & Li, Y. (2019). Metallic catalysts for structure-controlled growth of single-walled carbon nanotubes. *Single-Walled Carbon Nanotubes: Preparation, Properties and Applications*, 25-67.
23. Hirotani, J., & Ohno, Y. (2019). Carbon nanotube thin films for high-performance flexible electronics applications. *Single-Walled Carbon Nanotubes: Preparation, Properties and Applications*, 257-270.
24. Jeon, I., Matsuo, Y., & Maruyama, S. (2018). Single-walled carbon nanotubes in solar cells. *Single-Walled Carbon Nanotubes: Preparation, Properties and Applications*, 271-298.
25. Jia, X., & Wei, F. (2019). Advances in production and applications of carbon nanotubes. *Single-Walled Carbon Nanotubes: Preparation, Properties and Applications*, 299-333.